



Glycine-fueled solution combustion synthesis: photocatalytic activity of bismuth oxide on the degradation of organic dye molecules in relation to differences in fuel-oxidant ratio

Yayuk Astuti^{a,*}, Fikrian Kasalji^a, Didik Setiyo Widodo^a, Hendri Widiyandari^b

^aChemistry Department, Faculty of Science and Mathematics, Diponegoro University, 50275 Semarang, (Central Java), Indonesia, emails: yayuk.astuti@live.undip.ac.id (Y. Astuti), fikrian.kasalji96@gmail.com (F. Kasalji), widodo.ds@live.undip.ac.id (D.S. Widodo)

^bPhysics Department, Faculty of Mathematics and Natural Sciences, Sebelas Maret University, 57126, Surakarta, (Central Java), Indonesia, email: hendriwidiyandari@staff.uns.ac.id

Received 24 February 2021; Accepted 4 August 2021

ABSTRACT

Bismuth oxide is a semiconductor metal oxide that can be synthesized by the solution combustion method. The purpose of this research is to synthesize bismuth oxide pertaining to variations in the fuel-oxidant ratio and determine the characteristics and the photocatalytic activity of bismuth oxide for the degradation of organic dye molecules including remazol black B, methyl orange and rhodamine B. The resulting products synthesized with the three ratios $\phi > 1$, $\phi = 1$, and $\phi < 1$ were in the form of yellow powder. Fourier-transform infrared spectroscopy results of the three samples showed the presence of Bi–O–Bi and Bi–O functional groups indicating that Bi₂O₃ was formed. Moreover, X-ray diffractogram indicated that Bi₂O₃ particles contained in all samples were a mixture of α -Bi₂O₃ and β -Bi₂O₃ phases. Coral reef-like morphology was observed in all samples with Bi₂O₃ $\phi = 1$ having the smallest particle size followed by $\phi > 1$ and $\phi < 1$. Furthermore, Bi₂O₃ with $\phi > 1$, $\phi = 1$, and $\phi < 1$ have band gaps of 2.584, 2.581 and 2.625 eV, respectively. The photocatalytic activity test showed that bismuth oxide synthesized with the ratio $\phi = 1$ showed the best photocatalytic activity compared to $\phi > 1$ and $\phi < 1$ in the three different organic dye molecules, namely remazol black B, methyl orange, and rhodamine B.

Keywords: Bismuth oxide; Solution combustion; Photocatalysis; Photocatalyst; Fuel-oxidant; Glycine

1. Introduction

Bismuth oxide semiconductor material can be applied in various forms including solid oxide fuel cells [1], gas sensors [2], high temperature superconducting materials [3], functional ceramics [4] and photocatalysts [5]. The advantages it possesses include electrical and optical properties, wide range band-gap (2–3.89 eV), high refractive index ($n\delta\text{Bi}_2\text{O}_3$) and high dielectric permittivity ($\epsilon_r = 190$) [6]. The semiconductor properties and band gap values in bismuth oxide are of interest for use as photocatalyst in degrading organic pollutants under UV light. Bismuth

oxide has been found to have 6 morphological forms, namely α -Bi₂O₃, β -Bi₂O₃, γ -Bi₂O₃, ω -Bi₂O₃, and ϵ -Bi₂O₃ [7].

Bismuth oxide can be synthesized by various methods, including hydrothermal [8], deposition [9], precipitation [10,11], solution combustion [12–14] and sol–gel methods [15,16]. The solution combustion method in this research was chosen because it has advantages such as fast and easy working time, greater homogeneity, high purity, and small particle size formation [17]. The solution combustion method is a synthesis method in which it involves main components consist of oxidant and fuel with processes involving high temperatures [18]. The fuel used in

* Corresponding author.

this solution combustion method acts as a reducing agent in water-soluble substances [19]. Glycine, sucrose, urea, and citric acid are fuels normally applied in the solution combustion method [18]. The fuel chosen in this research was glycine. Glycine was used for two purposes, firstly to provide C and H in the combustion process and secondly to equip the breaking of various metal ion complexes with $-\text{NH}_2$ and the $-\text{COOH}$ groups, to prevent selective precipitation in maintaining the homogeneity of the composition [19].

Factors influencing synthesis of bismuth oxide using the solution combustion method include the ratio of fuel-oxidant, temperature, types of flame, and the amount of gas produced. In this research, a variation in the fuel-oxidant ratio (ϕ) was performed. The effect of the ratio of fuel-oxidant on the resulting products was determined. The properties affected by the fuel-oxidant ratio are morphology, crystal structure, and particle size. These properties affect the photocatalytic activity of the resulting bismuth oxides upon degradation of dye molecules.

Liu et al. [20] reported the synthesis of ZnFe_2O_4 as an anode material for lithium ion batteries using the solution combustion method with glycine as fuel. The variation of fuel-oxidant ratio applied were 0.5; 1; 1.5. The results indicated the higher the ratio of glycine to nitrate, the higher the number of pores. Moreover, the best crystallinity was obtained in the ratio of 1. The results showed that in ratio 1, pure ZnFe_2O_4 was produced with various structures and fewer residues due to the release of a lot of heat in the combustion process. Salunkhe et al. [21] reported the synthesis of cobalt ferrite (CoFe_2O_4) using the solution combustion method with glycine as fuel. The ratios of fuel-oxidant were varied, that is, 2.22, 1.48 and 0.74. The results revealed that increase in the fuel-oxidant ratio led to the increase in the amount of gas produced. Further, it affected the size of the crystal grains and the formation of the material structures. Astuti et al. [22] reported the effect of the ratio of citric acid (fuel)-bismuth nitrate pentahydrate (oxidant) on the photocatalytic activity of bismuth oxide prepared by the solution combustion method. The results showed that the ratio of $\phi > 1$ resulted in a product with the highest photocatalytic activity than $\phi = 1$, and $\phi < 1$. La et al [23] researched on nano- Bi_2O_3 powder synthesized by this method using bismuth nitrate as the oxidant and citric acid as the fuel. The research focused on the effects of temperature and fuel-oxidant ratio on the phase transformation, morphology, and particle size of the nano- Bi_2O_3 . The ratio of 6:5 resulted in smaller particle than the ratios of 6:3, 6:7 and 6:9. Bi_2O_3 nanoparticles as small as 10.7 nm had been able to be prepared using 0.005 moles of citric acid as fuel and 0.04 g of PEG-20000 as dispersants. Therefore, this research aims to investigate the effect of fuel oxidant ratio on the physicochemical properties and photocatalytic activity of bismuth oxide prepared by the glycine-fueled solution combustion method.

In this research, the effect of fuel oxidant ratio on the structural characteristics of Bi_2O_3 was investigated and evaluated. Moreover, the photocatalytic activity of the resulting product was determined by through their application in dye molecules degradations. The fuel-oxidant ratio variations prepared were $\phi = 1.2$; $\phi = 1$; dan $\phi = 0.8$. The resulting products were characterized using Fourier-transform infrared

spectroscopy (FTIR), X-ray diffraction (XRD), differential reflectance spectroscopy-ultraviolet (DRS-UV), scanning electron microscopy (SEM) and TGA-DTA. Additionally, the resulting products were applied to degrade organic dye molecules as pollutant models. The dyes chosen were remazol black B, methyl orange, and rhodamine B which are commonly applied for coloring in Batik Industry. These three compounds are dyes that have azo groups ($-\text{N}=\text{N}-$) bound to substituted aromatic rings which have high toxicity against organisms.

2. Experimental

2.1. Materials

The materials used in this research were bismuth nitrate pentahydrate (Sigma-Aldrich), glycine (Merck), nitric acid (Merck), remazol black B (RBB) (Merck), methyl orange (MO) (Merck), rhodamine B (RhB) (Merck), and distilled water.

2.2. Research procedures

2.2.1. Synthesis of bismuth oxide using the solution combustion method

2.42 g of bismuth nitrate pentahydrate at $\phi = 1$ was dissolved in 10 mL of HNO_3 0.04 M which was then added with 0.025 g of glycine. The mixture was then stirred at 400 rpm using a stirrer (cimarec SP131320–33Q) for 5 min until the entire solution became homogeneous. The solution was then heated at 300°C for 8 h. The formed product was then calcined in a furnace (Eurotern 2116) for 4 h at 700°C . This procedure was also applied for bismuth oxide synthesized with $\phi = 0.8$ and $\phi = 1.2$, that is, the mass of bismuth nitrate pentahydrate were 1.94 and 2.91 g, respectively. The products produced from $\phi = 0.8$, 1, and 1.2 before calcination were labelled BO1, BO2, BO3 respectively. While, after calcination, they were consecutively labelled as BO4, BO5, and BO6.

2.2.2. Product characterization

The resulting products were characterized using FTIR, XRD, DRS-UV, and SEM instruments. The functional groups present in the samples were analyzed using FTIR instrument, Shimadzu Irfinnity-1, at a wavelength range of $400\text{--}4,000\text{ cm}^{-1}$. The crystal structure was identified using XRD (D2 Phaser Bruker) with a $\text{CuK}\alpha$ radiation source, a wavelength of 1.54178 \AA X-Ray radiation, an electric current of 30 mA, a voltage of 30 kV and a 2θ range of 10° to 90° . The diffractogram patterns were then compared with the Joint Committee on Powder Diffraction Standards (JCPDS) for bismuth oxide. Furthermore, the band gap and morphology of the products were analyzed using DRS-UV (UV Cary 60 Agilent) and SEM (JOEL 6510 LA) with 20 kV with morphological magnifications of 250, 500 and 1,000.

2.2.3. Photocatalytic activity test of bismuth oxide

The organic dye molecule solutions were prepared with at a concentration of 5 ppm for MO and RhB, and 25 ppm for RBB. 50 mL of each dye solution was added

with 1 g of bismuth oxide which was then photocatalyzed using a UV-A light. The time variations of the photocatalysis were 1, 2, 3, 4, and 5 h of irradiation for RBB and RhB, while for MO they were 2, 4, 6, 8, and 10 h. After the photocatalysis, each solution was then centrifuged to separate out the bismuth oxide. Each solution was then analyzed using a UV-VIS spectrophotometer (Shimadzu UV-1280) to observe the absorbance value. The concentrations of the dye solutions at time t were calculated by comparing with the standard curve of each dye. Meanwhile, percent degradation of dyes after the photocatalysis under different time variations was calculated based on Patil et al. [24] using the following equation:

$$\text{Percent degradation} = \left(\frac{C_o - C_t}{C_o} \right) \times 100\% \quad (1)$$

where C_o is the initial concentration of the dye, while C_t is the concentration of the dye at time t .

3. Results and discussion

3.1. Synthesis of bismuth oxide

The starting material, bismuth nitrate pentahydrate ($\text{Bi}(\text{NO}_3)_3 \cdot 5\text{H}_2\text{O}$) was used as an oxidant, that is, provider

of oxygen that also helps in combustion [18]. Alternatively, the fuel used acted as a reducing agent. The fuel used was glycine containing C–H bonds [18]. The molar ratios between bismuth nitrate pentahydrate and glycine of 1.2, 1, 0.8 were used to control the final material properties [25].

The formed solution was heated at 300°C for 8 h, producing CO_2 , N_2 and H_2O gasses [26]. The products after heating for 8 h can be seen in Fig. 1. All three pictures show a yellow product which means that bismuth oxide had formed. Contrarily, white coloring in the product signifies that there was still bismuth nitrate pentahydrate which had not transformed and black indicates the presence of carbon in the sample from glycine (CH bond). Considerable difference among the products can be observed in $\phi = 1.2$ which had more orange and black colors from the CH due to higher use of fuel.

The products obtained after calcination for 4 h at a temperature of 700°C can be seen in Fig. 2. The three products obtained had the same yellow color with the weight of the BO3, BO2, BO1 of 1.022, 0.916 and 0.688 g, respectively.

The yellow color in the product indicates that bismuth oxide was formed [27]. This is one of the physical properties of bismuth oxide produced by the absorption of the visible light radiation in the wavelength range of 400–700 nm. Bismuth oxide is a semiconductor that generally has comparatively greater energy or shorter wavelengths

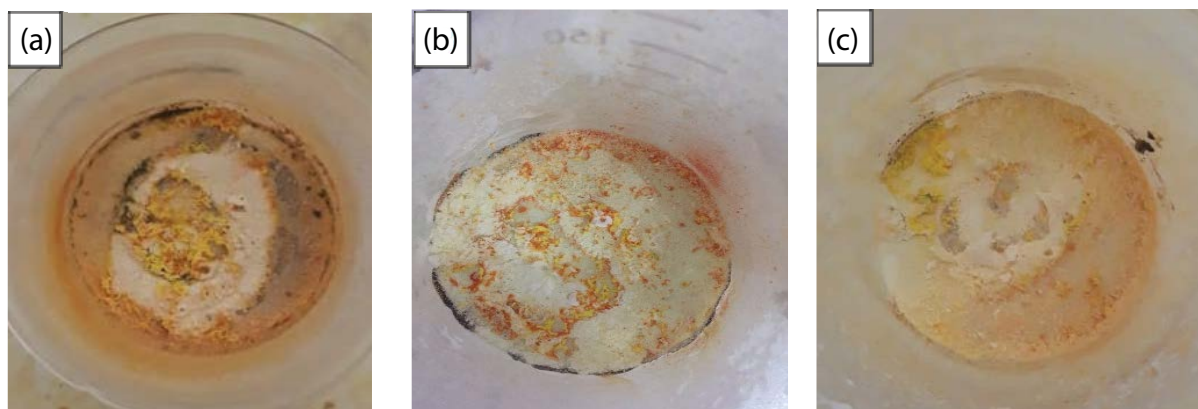


Fig. 1. Bismuth oxide powders synthesized after heating for 8 h: (a) BO1, (b) BO2, and (c) BO3.

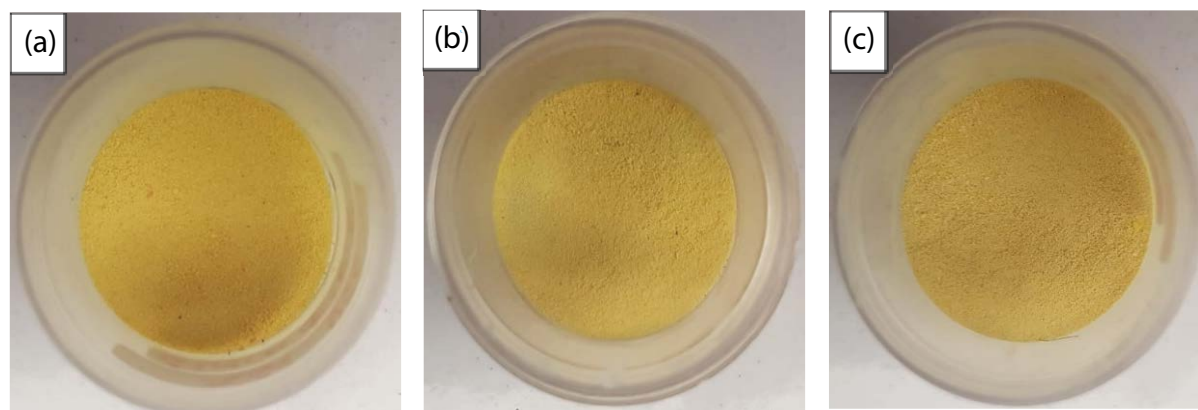


Fig. 2. Bismuth oxide powders after calcination for 4 h: (a) BO3, (b) BO4, and (c) BO5.

compared to other materials. Bismuth oxide has a band gap value of 2.3–3 eV, which means it can absorb light beams with greater energy, namely the blue and violet lights (2.5–3 eV). Blue and violet beams of light when absorbed appear yellow [28].

Material synthesis using the solution combustion method can generate metal oxides from the metal nitrates decomposition and fuel oxidation reactions. In addition to the formation of bismuth oxide, gases are also produced, namely CO_2 , N_2 and H_2O [29].

3.2. Characterization of bismuth oxide

3.2.1. Fourier-transform infrared spectroscopy

Figs. 3 and 4 present FTIR spectra of products before and after calcination. In these spectra, the spectrum of pure bismuth oxide [14] is also presented for comparison. Peaks observed at 542, 539, and 544 cm^{-1} for BO1, BO2 and BO3, respectively, indicate the presence of Bi–O–Bi bond [30]. Vibration modes at 1,358, 1,381 and 1,358 cm^{-1} attributed to Bi–O functional groups were observed also in the three products. However, the intensity of these vibration modes were higher in products before calcination. The high intensity was due to the presence of NO_3^- [31], even though this functional group is also attributed to Bi–O. This functional group disappeared after heating at calcination beyond the boiling point of NO_3^- at 380°C [32]. Therefore, after calcination the intensity of these vibration modes decreased.

Fig. 4 shows the FTIR spectra of products after calcination. Peaks observed at 508, 507 and 508 cm^{-1} for BO4, BO5

and BO6, signifies Bi–O–Bi bonds [30] and vibration modes at 1,381, 1,383 and 1,384 cm^{-1} indicate the presence of the stretching mode of Bi–O [30]. These results verified that in each ratio, Bi_2O_3 had been formed.

3.2.2. X-ray diffraction

X-Ray diffractograms shown in Fig. 5 present the products after calcination containing 2 types of crystalline structures, $\alpha\text{-Bi}_2\text{O}_3$ (monocyclic) and $\beta\text{-Bi}_2\text{O}_3$ (tetragonal). The existence of $\alpha\text{-Bi}_2\text{O}_3$ is indicated by peaks at 2θ values of 27.04°, 27.50°, and 33.27° for BO6, 26.89°, 27.38°, and 33.23° for BO5, and 27.01°, 27.48°, and 33.32° for BO4. These peaks correspond to the database in JCPDS number 41-1449 for $\alpha\text{-Bi}_2\text{O}_3$.

The existence of $\beta\text{-Bi}_2\text{O}_3$ is indicated by the presence of peaks at 2θ of 25.87°, 46.43°, and 55.61° for BO6, 25.73°, 46.30°, and 55.80° for BO5, and 25.88°, 46.40°, and 55.58° for BO4. These peaks correspond to the database in JCPDS number 27-0050 for $\beta\text{-Bi}_2\text{O}_3$.

3.2.3. Differential reflectance spectroscopy-ultraviolet

Fig. 6 shows the results of DRS-UV of BO4, BO5 and BO6 products. The band gap values of BO6, BO5 and BO4 observed were 2.584, 2.581 and 2.625 eV, respectively. BO5 had the lowest band gap, meanwhile the band gaps of BO5 and BO6 were almost the same. Bedoya Hincapie et al. [33] reported the values of band gap for $\alpha\text{-Bi}_2\text{O}_3$ and $\beta\text{-Bi}_2\text{O}_3$ of 2.85 and 2.58 eV, respectively. Crystal composition consisting of $\alpha/\beta\text{-Bi}_2\text{O}_3$ will have decreased band gap value from the band gap value of just $\alpha\text{-Bi}_2\text{O}_3$.

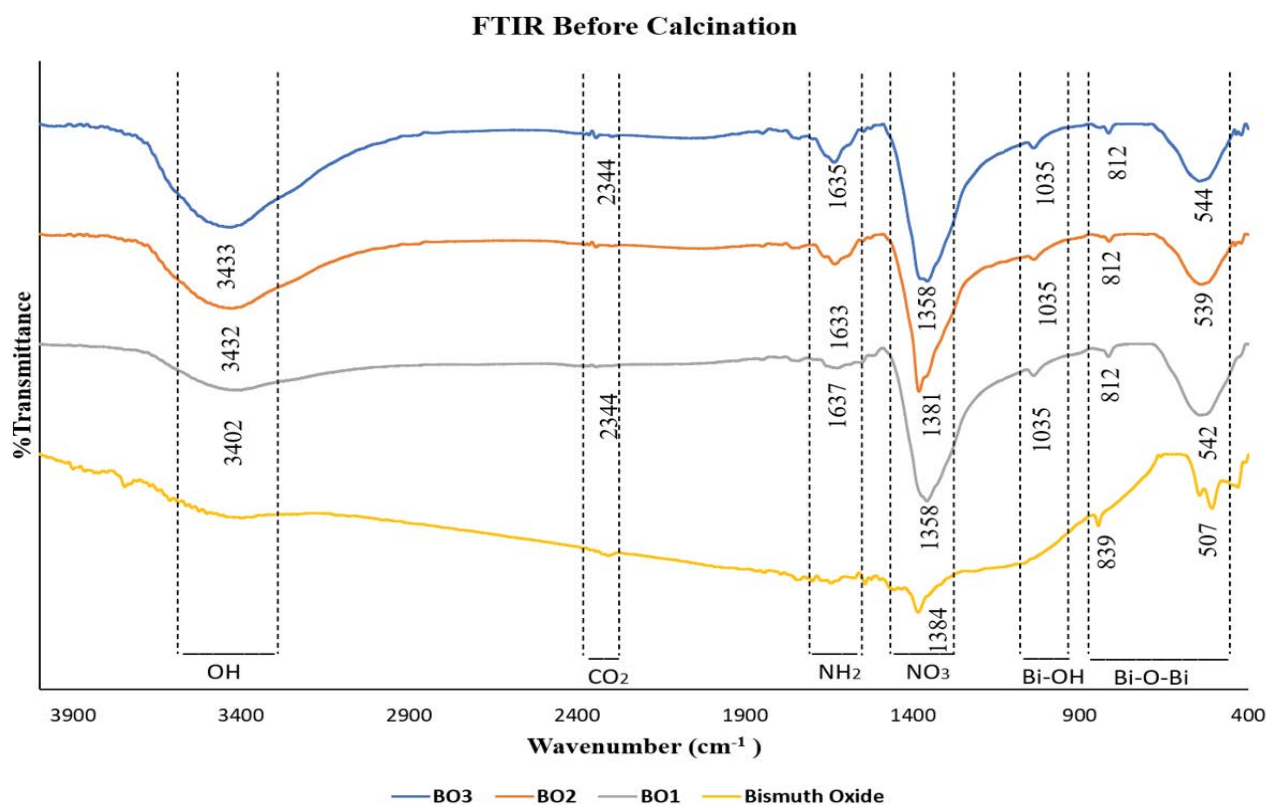


Fig. 3. FTIR spectra of the samples before calcination.

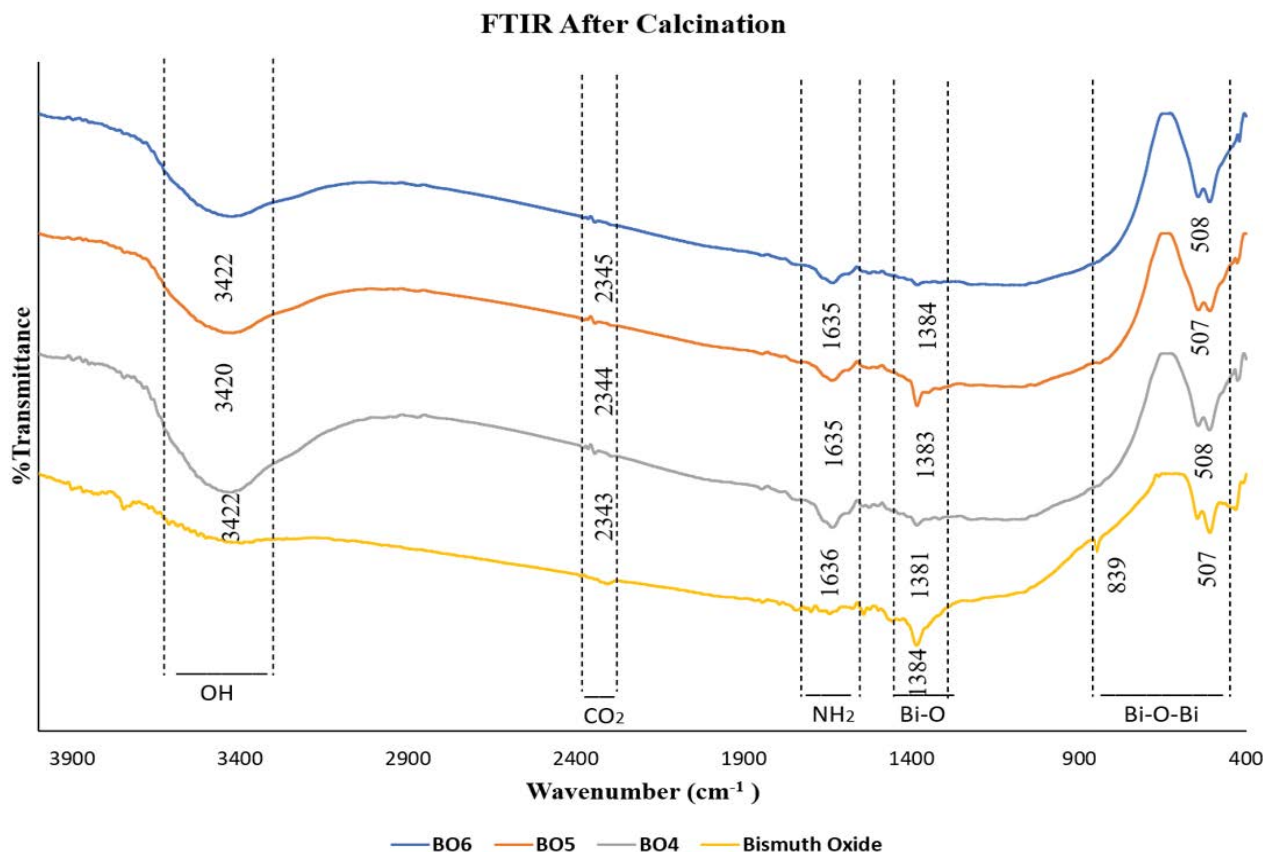


Fig. 4. FTIR spectra of the samples after calcination.

3.2.4. Scanning electron microscopy

The morphologies of the products are presented in Fig. 7. All products have irregular coral reefs-like shapes. In addition to their morphologies, the diameter of the crystallite size was also calculated using the ImageJ software. The smallest diameter range was shown by BO5; meanwhile the largest diameter range belonged to BO4 as presented in Table 1.

The large particles in BO6 and BO4 were due to agglomeration of particles. In BO5, smaller particle diameters were observed as the ratio of fuel to oxidant was equal to 1 ($\phi = 1$). The reaction that occurred is in accordance with the stoichiometry so that the solution combustion reaction occurred optimally [20,29,34]. Particle size in BO6 was observed to be dominated by particles of 65.06 micrometers in size. In BO4, particles with a size of 71.89 μm were also more dominant than other sizes. In contrast, in BO5, small particles dominate.

3.3. Photocatalytic activity of bismuth oxide

In this study bismuth oxides synthesized by the solution combustion method were tested for their photocatalytic activity in degrading remazol black B (RBB), methyl orange (MO) and rhodamine B (RhB) dyes. The test was carried out by varying the duration of light irradiation for each dye. The absorbance of this dye solution was measured using a UV-Vis spectrophotometer.

In the photocatalysis process, the longer the irradiation time, the more photons will hit the system. Fig. 8a shows the photocatalytic degradation of RBB in which BO5 had the highest percentage of degradation at 77.52%, followed by BO6 at 39.6% and BO4 at 34.8%. Meanwhile, in the photocatalytic degradation of MO, as seen in Fig. 8b, BO5, again, had the highest percentage of degradation at 99.18%, followed by BO6 at 92.2% and BO4 at 61.16%. In the photocatalysis degradation of RhB (Fig. 8c), BO5 was most effective in degrading the dye compared to as seen from the percent degradations of 71.11%, 61.45% and 51.58% for BO5, BO6 and BO4, respectively.

In order to prove that BO4, BO5 and BO6 have no activity without light, three dyes were mixed with them and treated without light irradiation for 30 min for all dyes and further 10 h for MO and 5 h for RBB and RhB. Table 2 shows that without light irradiation, the absorbances of the dyes are higher than that of dyes solution with light irradiation.

In this study, the kinetics of the dye degradation process by the three bismuth oxide samples synthesized at different fuel/oxidant ratios were studied. According to Wang et al. [6] the degradation of dyes generally follows the first order reaction kinetics expressed as follows:

$$\ln C_t = \ln C_o - kt \quad (2)$$

where C_o = initial concentration of solution (ppm), C_t = concentration of solution (ppm) at time t , and k = reaction rate constant in the first order (s^{-1}).

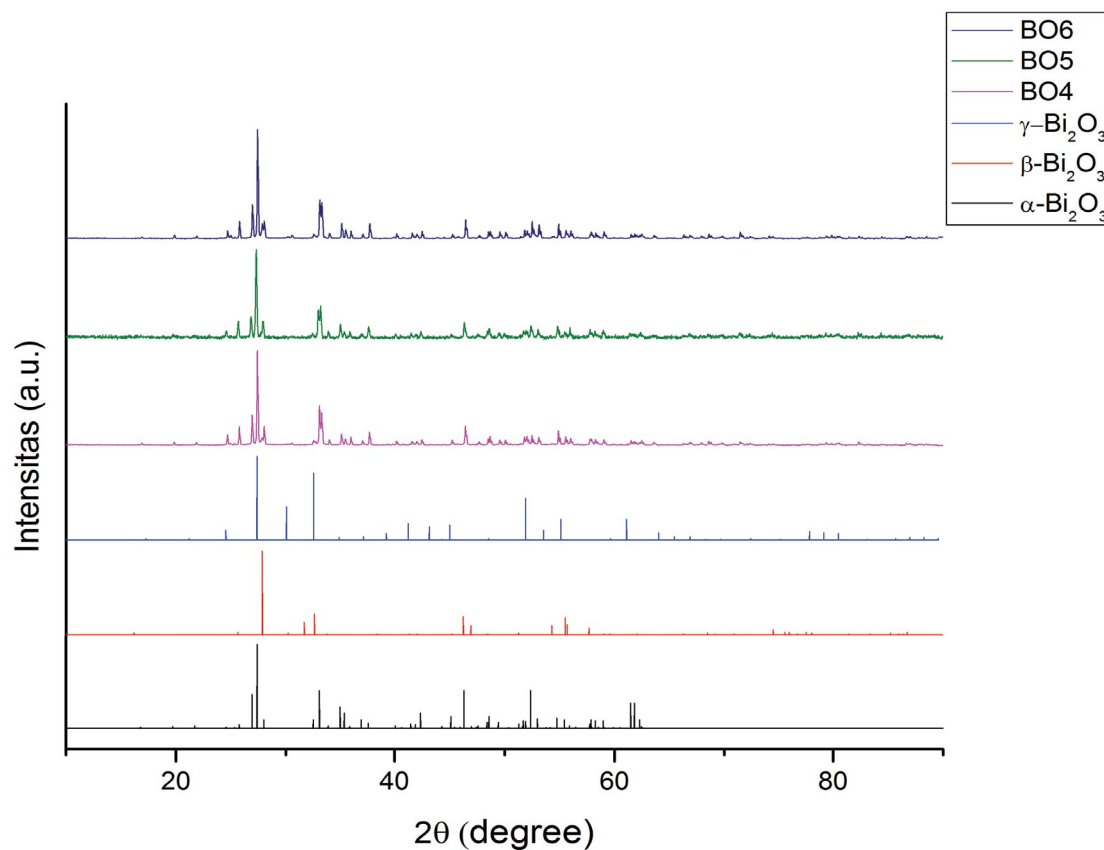


Fig. 5. XRD diffractogram of the synthesized bismuth oxides.

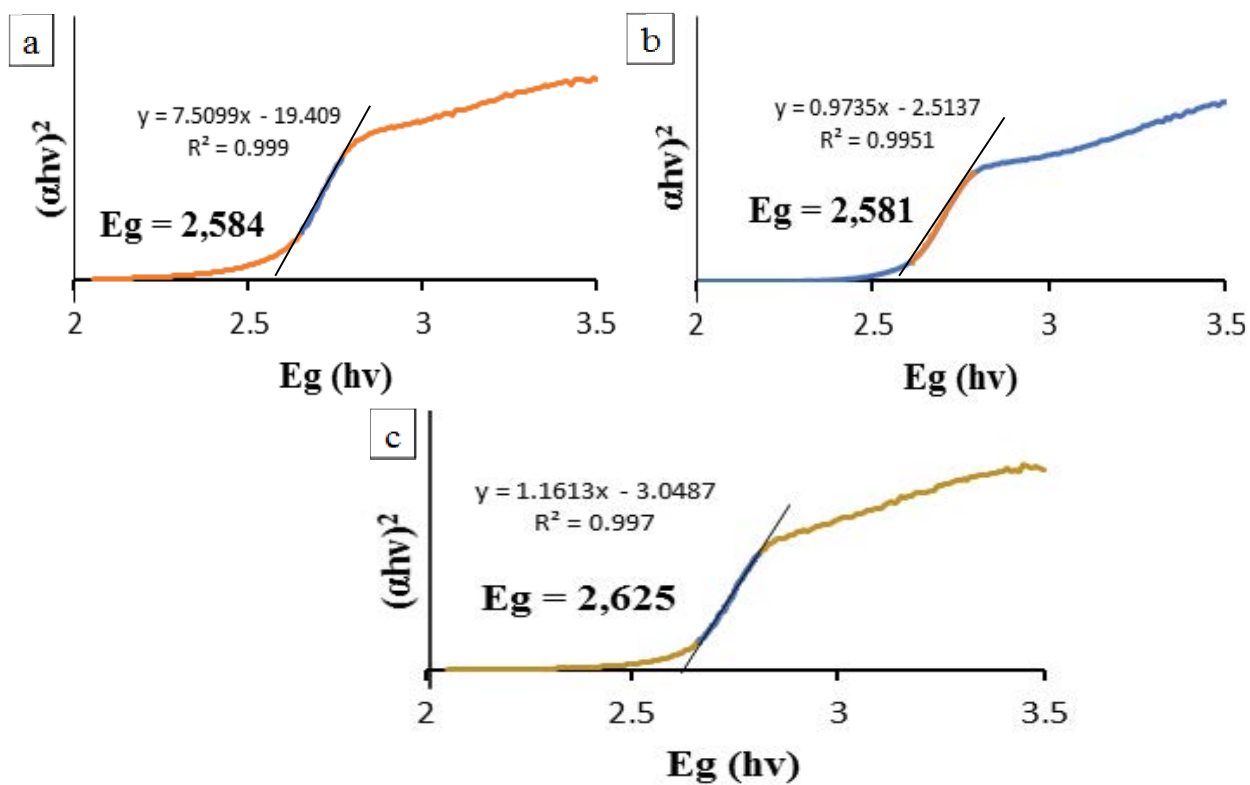


Fig. 6. DRS-UV graph of bismuth oxide synthesized with glycine fuel: (a) BO6, (b) BO5, and (c) BO4.

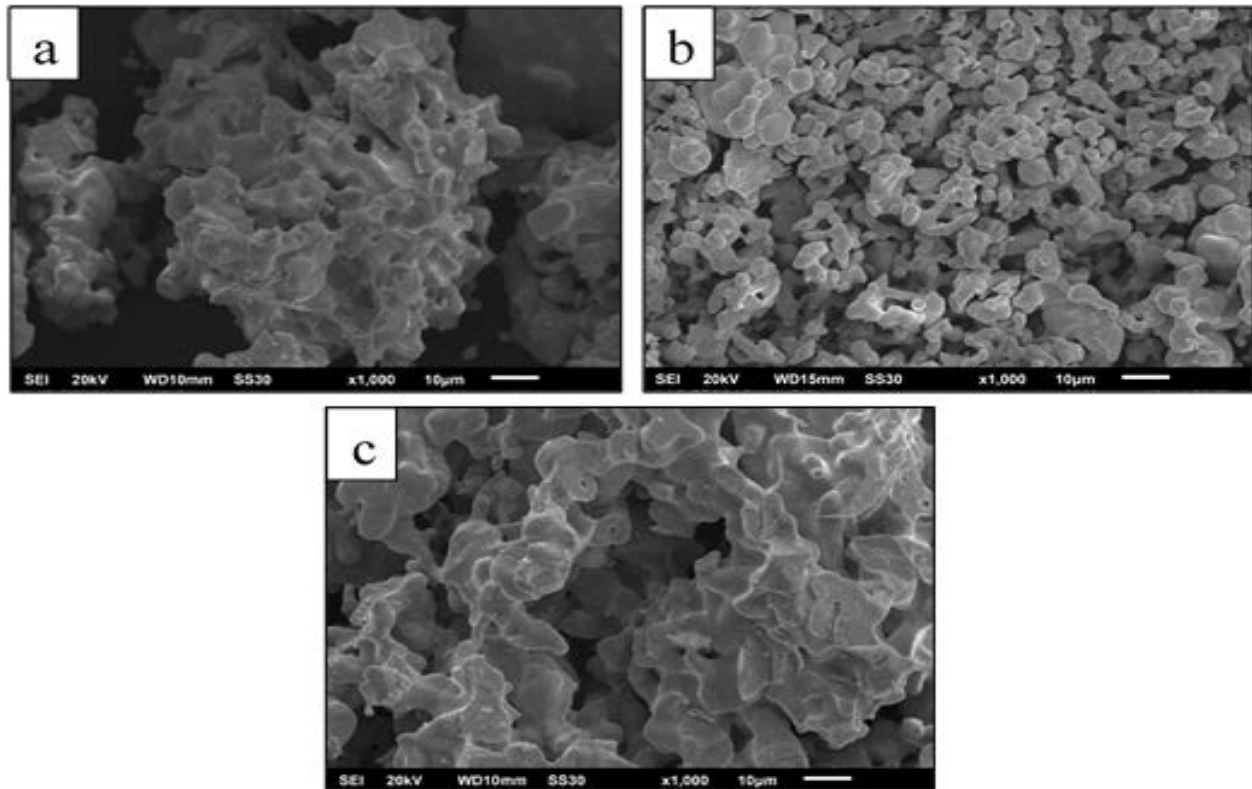


Fig. 7. SEM images of bismuth oxides with variations in fuel/oxidant: (a) BO6, (b) BO5, and (c) BO4 at 1,000x magnification.

Table 1
Diameter ranges of bismuth oxide particles synthesized by solution combustion

Fuel/oxidant ratio	Particle diameter (μm)
BO6	3.03–65.06
BO5	0.91–21.07
BO4	3.08–71.89

Fig. 9a shows the measured kinetics of the degradation of remazol black B which follows the first order reaction. Based on the linear equation, the slope signifies k . The highest k was obtained in BO5, that is $7.54 \times 10^{-5} \text{ s}^{-1}$, followed by BO6 and BO4 with values of $2.62 \times 10^{-5} \text{ s}^{-1}$ and at $2.41 \times 10^{-5} \text{ s}^{-1}$. Fig. 9b shows the degradation kinetics of methyl orange which also follows the first order kinetics. The highest constant value obtained from BO5, BO6 and BO4 were $13.4 \times 10^{-5} \text{ s}^{-1}$, $6.89 \times 10^{-5} \text{ s}^{-1}$ and $2.76 \times 10^{-5} \text{ s}^{-1}$. The degradation kinetics of rhodamin B is depicted in Fig. 9c. The smallest reaction rate constant value was obtained from BO4, followed by BO6 $3.41 \times 10^{-5} \text{ s}^{-1}$, $4.89 \times 10^{-5} \text{ s}^{-1}$, while the highest rate constant was obtained from BO5 with the value of $5.77 \times 10^{-5} \text{ s}^{-1}$. The photocatalytic activity tests on the 3 dye molecules demonstrated that BO5 has the highest reaction rate constant, followed by BO6 and BO4. The value obtained is related to the characteristics of the bismuth oxide synthesized.

Photocatalytic activity can be influenced by several characteristics of the bismuth oxide produced. The

diffraction patterns of the products (Fig. 5) show that the products mostly contained 2 crystal structures namely $\alpha\text{-Bi}_2\text{O}_3$ and $\beta\text{-Bi}_2\text{O}_3$. Photocatalytic activity of $\beta\text{-Bi}_2\text{O}_3$ is better than $\alpha\text{-Bi}_2\text{O}_3$ because it has smaller band gap. However, when combined into a crystal structure consisting of $\alpha/\beta\text{-Bi}_2\text{O}_3$, the consequent material will have photocatalytic activity that is more effective and efficient [35]. The $\alpha/\beta\text{-Bi}_2\text{O}_3$ composition contained in the product increased the separation of electron hole caused by electron transfer. Therefore, this product showed the highest photocatalytic activity than products consisting of only one phase of $\beta\text{-Bi}_2\text{O}_3$ alone [36]. In order to see the differences in the characteristics of the synthesized products in terms of the effect on photocatalytic activity, crystal structure alone would not suffice. Other characterization, namely the absorbance of the functional groups, band gap value, and the crystalline morphology, are also needed.

The IR spectra results of the products can be seen in Figs. 3 and 4. The intensity of the Bi–O peak group on the synthesized products can indicate the concentration of the bismuth oxide formed. Spalding et al. [37] reported that the higher the intensity of the group formed, the higher the concentration of the group. Thus, the higher intensity, and consequently higher concentration of the Bi–O group contained in Bi_2O_3 was deduced to have increased bismuth oxide activity as a photocatalyst. Looking at the photocatalyst activities in the degradation of RBB, MO and RhB, BO5 had the largest photocatalyst activity, then BO6 and BO4.

The DRS-UV results (Fig. 6) show that BO5 had a lower band gap value, followed by BO6 and BO4. Labib [38]

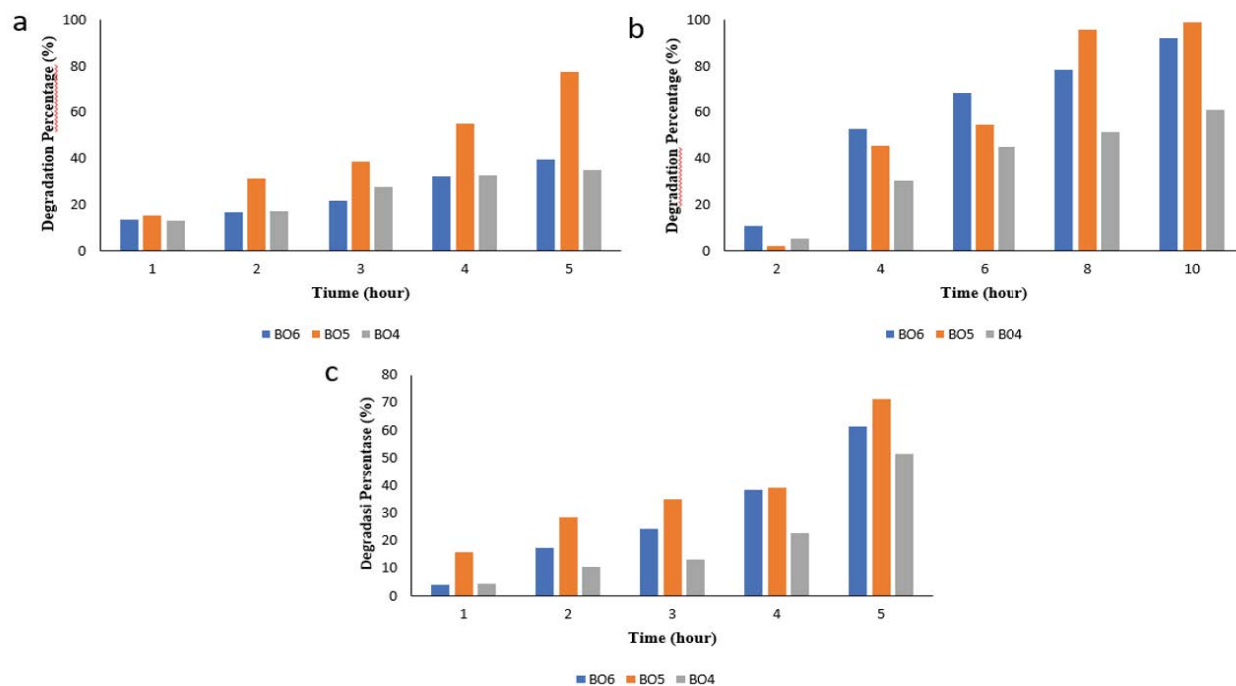


Fig. 8. Percent degradation of (a) RBB, (b) MO, and (c) RhB dyes in relation to duration of photocatalysis.

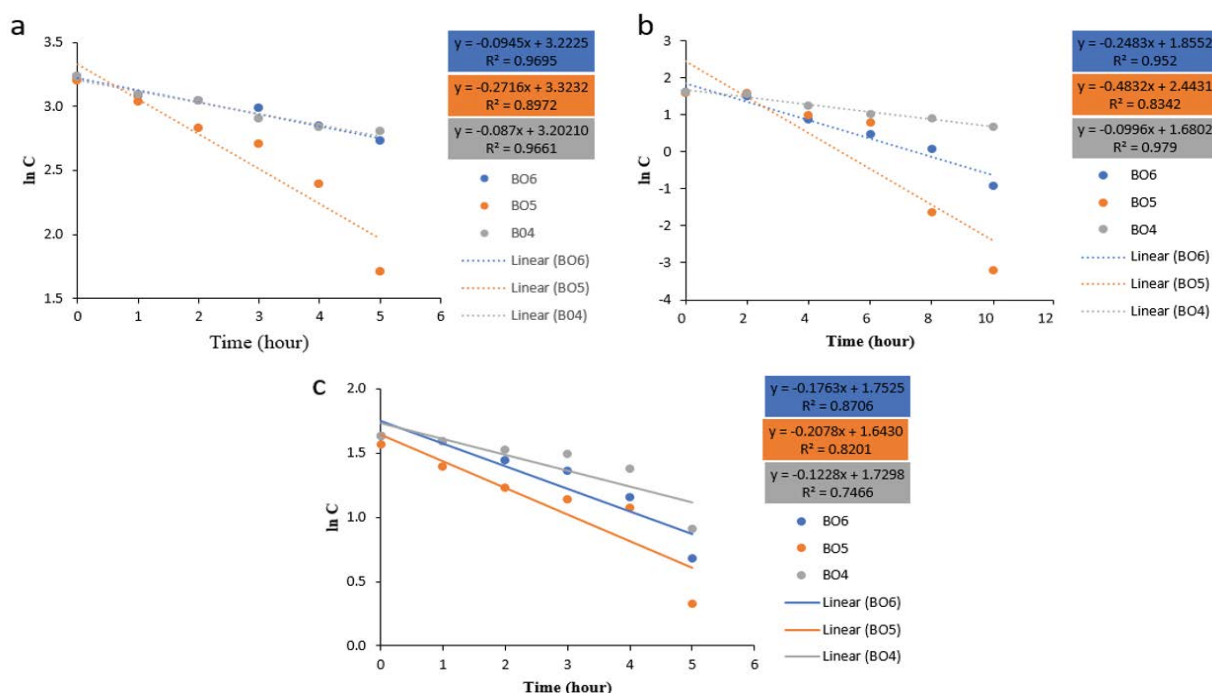


Fig. 9. First-order photocatalytic degradation of (a) RBB, (b) MO, and (c) RhB.

reported that the smaller the band gap, the better the photocatalytic activity. A small band gap small will prompt absorption of light with large wavelength, thereby increasing photocatalyst activity. This is consistent with the results of the photocatalytic activity of RBB, MO and RhB solutions whereby the greatest value was found at BO5, then followed by BO6 and BO4.

Furthermore, observed through SEM images seen in Fig. 7, the smaller the particle size, the greater the surface area. The diameter range of three products can be seen in Table 1. A product that has a large surface area will have increased photocatalyst activity because the photocatalyst and the dye molecules will have greater surface to interact more frequently. From the SEM images, it was found that

Table 2
The absorbance of dyes after being mixed with BO4, BO5 and BO6 without light irradiation

Dyes Solution	Samples	Absorbances	
		30 min	5/10 h
MO	BO6	0.361	0.314
	BO5	0.385	0.311
	BO4	0.378	0.315
RBB	BO6	0.530	0.436
	BO5	0.471	0.424
	BO4	0.529	0.459
RhB	BO6	0.485	0.392
	BO5	0.467	0.415
	BO4	0.477	0.433

BO5 had the smallest diameter, followed by BO6 and BO4. This is consistent with the photocatalytic activity data in which BO5 showed the highest photocatalytic activity rate constant in the degradation of RBB MO and RhB solutions, followed by BO6 and BO4.

4. Conclusion

Variations in the fuel-oxidant ratio in the glycine-fueled solution combustion synthesis of bismuth oxide affect the photocatalytic activity of the bismuth oxide produced against methyl orange, rhodamine B and remazol black B organic dyes to be different. The product generated from the use of fuel-oxidant ratio of 1 showed the best photocatalytic activity for the degradation of the three dye molecules as indicated by the degradation rate constant. The difference in photocatalytic activity among the products is related to the crystal structure, band gap, and the morphology of the particles.

Acknowledgments

The authors would like to thank the Ministry of Research, Technology and Higher Education for the funding support provided for this research through “Penelitian Dasar” scheme in the fiscal year of 2018 (No. 101-71/UN7.P4.3/PP/2018) and 2019 (No. 101-71/UN7.P4.3/PP/2019).

References

- [1] O. Monnereau, L. Tortet, P. Llewellyn, F. Rouquerol, G. Vacquier, Synthesis of Bi_2O_3 by controlled transformation rate thermal analysis: a new route for this oxide?, *Solid State Ionics*, 157 (2003) 163–169.
- [2] S.S. Bhande, R.S. Mane, A.V. Ghule, S.H. Han, A bismuth oxide nanoplate-based carbon dioxide gas sensor, *Scr. Mater.*, 65 (2011) 1081–1084.
- [3] N.V. Skorodumova, A.K. Jonsson, M. Herranen, M. Strømme, G.A. Niklasson, B. Johansson, S.I. Simak, Random conductivity of $\delta\text{-Bi}_2\text{O}_3$ films, *Appl. Phys. Lett.*, 86 (2005) 241910, doi: 10.1063/1.1948516.
- [4] M.A. De la Rubia, M. Peiteado, J.F. Fernandez, A.C. Caballero, Compact shape as a relevant parameter for sintering $\text{ZnO-Bi}_2\text{O}_3$ based varistors, *J. Eur. Ceram. Soc.*, 24 (2004) 1209–1212.
- [5] L. Zhang, W. Wang, J. Yang, Z. Chen, W. Zhang, L. Zhou, S. Liu, Sonochemical synthesis of nanocrystallite Bi_2O_3 as a visible-light-driven photocatalyst, *Appl. Catal., A*, 308 (2006) 105–110.
- [6] Y. Wang, J. Zhao, Z. Wang, A simple low-temperature fabrication of oblique prism-like bismuth oxide via a one-step aqueous process, *Colloids Surf., A*, 377 (2011) 409–413.
- [7] Y. Polat, Comments on “Reduced band gap & charge recombination rate in Se doped $\alpha\text{-Bi}_2\text{O}_3$ leads to enhanced photoelectrochemical and photocatalytic performance: theoretical & experimental insight”, *Int. J. Hydrogen Energy*, 42 (2017) 20638–20648.
- [8] C. Wu, L. Shen, Q. Huang, Y.C. Zhang, Hydrothermal synthesis and characterization of Bi_2O_3 nanowires, *Mater. Lett.*, 65 (2011) 1134–1136.
- [9] R. Hernandez-Delgadillo, D. Velasco-Arias, J.J. Martinez-Sanmiguel, D. Diaz, I. Zumeta-Dube, K. Arevalo-Niño, C. Cabral-Romero, Bismuth oxide aqueous colloidal nanoparticles inhibit *Candida albicans* growth and biofilm formation, *Int. J. Nanomed.*, 8 (2013) 1645, doi: 10.2147/IJN.S38708.
- [10] Y. Astuti, R. Andianingrum, A. Haris, A. Darmawan, The role of $\text{H}_2\text{C}_2\text{O}_4$ and Na_2CO_3 as precipitating agents on the physicochemical properties and photocatalytic activity of bismuth oxide, *Open Chem.*, 18 (2020) 129–137.
- [11] Y. Astuti, A.D. Wulansari, A. Haris, A. Darmawan, R. Balgis, Physicochemical properties and photocatalytic activity of bismuth oxide as affected by weak or strong base precipitants, *Songklanakarin J. Sci. Technol.*, 43 (2021) 608–614.
- [12] Y. Astuti, A. Fauziyah, S. Nurhayati, A.D. Wulansari, R. Andianingrum, A.R. Hakim, G. Bhaduri, Synthesis of α -bismuth oxide using solution combustion method and its photocatalytic properties, *IOP Conf. Ser.: Mater. Sci. Eng.*, 107 (2016) 012006.
- [13] Y. Astuti, D. Amri, D.S. Widodo, H. Widiyandari, R. Balgis, T. Ogi, Effect of fuels on the physicochemical properties and photocatalytic activity of bismuth oxide, synthesized using solution combustion method, *Int. J. Technol.*, 11 (2020) 26–36.
- [14] Y. Astuti, P.P. Elesta, D.S. Widodo, H. Widiyandari, R. Balgis, Hydrazine and urea fueled-solution combustion method for Bi_2O_3 synthesis: characterization of physicochemical properties and photocatalytic activity, *Bull. Chem. React. Catal.*, 15 (2020) 104–111.
- [15] M. Anilkumar, R. Pasricha, V. Ravi, Synthesis of bismuth oxide nanoparticles by citrate gel method, *Ceram. Int.*, 31 (2005) 889–891.
- [16] Y. Astuti, B.M. Listyani, L. Suyati, A. Darmawan, Bismuth oxide prepared by sol-gel method: variation of physicochemical characteristics and photocatalytic activity due to difference in calcination temperature, *Indones. J. Chem.*, 21 (2021) 108–117.
- [17] B.B. Das, A. Srinivassan, M. Yogapriya, M.R. Kongara, A. Punnoose, Sol-gel synthesis and characterization of $x\text{CuO-(1-x)Bi}_2\text{O}_3$ ($0.15 \leq x \leq 0.55$) glasses by magnetic and spectral studies, *J. Non-Cryst. Solids*, 427 (2015) 146–151.
- [18] A.K. Alves, C.P. Bergmann, F.A. Berutti, Novel Synthesis and Characterization of Nanostructured Materials, Springer, Berlin, 2016.
- [19] L.D. Jadhav, S.P. Patil, A.P. Jamale, A.U. Chavan, Solution combustion synthesis: role of oxidant to fuel ratio on powder properties, *Mater. Sci. Forum*, 757 (2013) 85–98.
- [20] J. Liu, D. Wang, P. Dong, J. Zhao, Q. Meng, Y. Zhang, X. Li, Effect of glycine-to-nitrate ratio on solution combustion synthesis of ZnFe_2O_4 as anode materials for lithium ion batteries, *Int. J. Electrochem. Sci.*, 12 (2017) 3741–3755.
- [21] A.B. Salunkhe, V.M. Khot, M.R. Phadatare, S.H. Pawar, Combustion synthesis of cobalt ferrite nanoparticles—influence of fuel to oxidizer ratio, *J. Alloys Compd.*, 514 (2012) 91–96.
- [22] Y. Astuti, A. Fauziyah, H. Widiyandari, D. Widodo, Studying impact of citric acid-bismuth nitrate pentahydrate ratio on photocatalytic activity of bismuth oxide prepared by solution combustion method, *Rasayan J. Chem.*, 12 (2019) 2210–2217.
- [23] J. La, Y. Huang, G. Luo, J. Lai, C. Liu, G. Chu, Synthesis of bismuth oxide nanoparticles by solution combustion method, *Part. Sci. Technol.*, 31 (2013) 287–290.

- [24] S.P. Patil, V.S. Shrivastava, G.H. Sonawane, S.H. Sonawane, Synthesis of novel Bi₂O₃–montmorillonite nanocomposite with enhanced photocatalytic performance in dye degradation, *J. Environ. Chem. Eng.*, 3 (2015) 2597–2603.
- [25] D. Levy, M. Zayat, *The Sol-Gel Handbook*, 3 Volume Set: Synthesis, Characterization and Applications, John Wiley & Sons, Weinheim, 2015.
- [26] K. Deshpande, A. Mukasyan, A. Varma, Direct synthesis of iron oxide nanopowders by the combustion approach: reaction mechanism and properties, *Chem. Mater.*, 16 (2004) 4896–4904.
- [27] N. Eastaugh, V. Walsh, T. Chaplin, R. Siddall, *Pigment Compendium: A Dictionary and Optical Microscopy of Historic Pigments (Colors Paint Art)*, Elsevier, 2008.
- [28] D.W. Richerson, *Modern Ceramic Engineering: Properties, Processing, and Use in Design*, CRC Press, Utah, 2005.
- [29] R. Branquinho, A. Santa, E. Carlos, D. Salgueiro, P. Barquinha, R. Martins, E. Fortunato, *Solution Combustion Synthesis: Applications in Oxide Electronics*, Chapter in *Developments in Combustion Technology*, InTechOpen, London, 2016.
- [30] S. Bandyopadhyay, A. Dutta, Thermal, optical and dielectric properties of phase stabilized δ-Dy-Bi₂O₃ ionic conductors, *J. Phys. Chem. Solids*, 102 (2017) 12–20.
- [31] W. Raza, M.M. Haque, M. Muneer, T. Harada, M. Matsumura, Synthesis, characterization and photocatalytic performance of visible light induced bismuth oxide nanoparticle, *J. Alloys Compd.*, 648 (2015) 641–650.
- [32] D.W. Barnum, Some history of nitrates, *J. Chem. Educ.*, 80 (2003) 1393.
- [33] C.M. Bedoya Hincapie, M.J. Pinzon Cardenas, J.E. Alfonso Orjuela, E. Restrepo Parra, J.J. Olaya Florez, Physical-chemical properties of bismuth and bismuth oxides: synthesis, characterization and applications, *Dyna*, 79 (2012) 139–148.
- [34] A. Varma, A.S. Mukasyan, A.S. Rogachev, K.V. Manukyan, Solution combustion synthesis of nanoscale materials, *Chem. Rev.*, 116 (2016) 14493–14586.
- [35] J. Hou, C. Yang, Z. Wang, W. Zhou, S. Jiao, H. Zhu, In situ synthesis of α-β phase heterojunction on Bi₂O₃ nanowires with exceptional visible-light photocatalytic performance, *Appl. Catal., B*, 142 (2013) 504–511.
- [36] T.A. Gadhi, A. Hernández-Gordillo, M. Bizarro, P. Jagdale, A. Tagliaferro, S.E. Rodil, Efficient α/β-Bi₂O₃ composite for the sequential photodegradation of two-dyes mixture, *Ceram. Int.*, 42 (2016) 13065–13073.
- [37] K. Spalding, F. Bonnier, C. Bruno, H. Blasco, R. Board, I. Benz-de Bretagne, H.J. Byrne, H.J. Butler, I. Chourpa, P. Radhakrishnan, M.J. Baker, Enabling quantification of protein concentration in human serum biopsies using attenuated total reflectance-Fourier transform infrared (ATR-FTIR) spectroscopy, *Vib. Spectrosc.*, 99 (2018) 50–58.
- [38] S. Labib, Preparation, characterization and photocatalytic properties of doped and undoped Bi₂O₃, *J. Saudi Chem. Soc.*, 21 (2017) 664–672.